

BOTTOM PHOTOGRAPHY AND SEDIMENT ANALYSES ON CESAR

C.L. Amos¹
Geological Survey of Canada

Amos, C.L., *Bottom photography and sediment analyses on CESAR*; in *Initial Geological Report on CESAR — the Canadian Expedition to Study the Alpha Ridge, Arctic Ocean*, ed. H.R. Jackson, P.J. Mudie and S.M. Blasco; Geological Survey of Canada, Paper 84-22, p. 25-45, 1985.

Abstract

An evaluation is made of the sediment transport pathways which lead to the accumulation of the bottom material in the vicinity of the Alpha Ridge. An estimate is also given of the sources of the material, the factors controlling deposition and, where appropriate, on the accumulation rates. Biogenic material, ice-rafted debris and weathered bedrock by-products make up the majority of the seabed sediment. The relative abundance of each component varies from the Alpha Ridge crest to the trough. Minor amounts of eolian-derived debris were detected in the pack ice and yet lower amounts of inorganic debris were measured in the water column.

Ice-rafted pebbles and cobbles were generally rounded and calcereous. Which suggests a source from a coastal region on the adjacent Canadian landmass.

The recovery of bedrock in the dredging program verifies the occurrence of outcrops on the south flank of the northern Alpha Ridge crest. The samples recovered are (1) well weathered basalts which have an elemental composition similar to floes sampled in the ice pack and water column, and (2) from fine grained sediment samples recovered from adjacent basins. A local bedrock source of bottom sediments had not hitherto been considered significant.

Résumé

Le rapport présente une évaluation des trajectoires suivies par les sédiments qui se sont accumulés sur le fond océanique aux alentours de la dorsale Alpha. Il évalue également les sources des matériaux, les facteurs contrôlant l'accumulation et, le cas échéant, les vitesses d'accumulation. La plupart des sédiments du fond océanique se composent de matériaux organogènes, de débris glaciels et de sous-produits de l'érosion du socle rocheux. L'abondance relative de chacune des composantes varie de la crête à la dépression de la dorsale Alpha. De petites quantités de débris éoliens ont été identifiées dans la banquise et des quantités encore plus réduites de débris inorganiques ont été décelées dans la colonne d'eau.

Les galets et les gros cailloux glaciels sont généralement arrondis et calcaires, ce qui porte à croire qu'ils proviennent d'une région côtière sur la masse continentale contiguë du Canada.

Les échantillons de socle rocheux prélevés par dragage confirment l'existence d'affleurements sur le flanc sud de la crête nord de la dorsale Alpha. Ces échantillons comportent (1) des basaltes fortement altérés dont la composition élémentaire est similaire à celle des flocons échantillonnés dans la banquise et dans la colonne d'eau et (2) des sédiments à grains fins provenant des bassins contigus. Une source locale de sédiments du fond dérivés du socle rocheux n'avait pas jusqu'ici été jugée importante.

¹Atlantic Geoscience Centre, Bedford Institute of Oceanography, Box 1006, Dartmouth, Nova Scotia, B2Y 4A2

INTRODUCTION

The sources of sediment comprising the unconsolidated Cenozoic sequence in the region of the Alpha Ridge have been speculated over, but no systematic analysis of the various sediment transport pathways had been made. Thus uncertainty remained over the depositional history of the region and the processes which control the lithology and rate of accumulation of the sequence.

The purpose of this study was to sample the particulate matter, both at the seabed and along the transport paths in order to determine sediment source, and to quantify, where possible, the contributions of each source to the sedimentary cover. This was achieved by adopting a number of accepted techniques such as filtration of the ice cover melt water and water column for particulate matter and subsequent elemental analysis using electron microscopy, by seabed sampling and photography, and by the application of sedimentation laws to the observations.

Due to the limitations imposed by drift rate, sampling strategy and breakdown, the data recovered were not necessarily representative of the region as a whole and therefore results should be considered only as a guide to the nature and origin of sediments at the Alpha Ridge. The results reported are tentative and may be subject to change as further analyses and interpretation are made.

ACKNOWLEDGMENTS

I thank Ruth Jackson, K.W. Asprey and H. Wiele for their support at the CESAR Camp, F. Cole for analysis of the microfauna and production of Plate 4.4, and P. Stoffyn for

assistance with SEM work and EDAX analysis. Ruth Jackson, Peta Mudie, D.J.W. Piper and S. Bell reviewed this manuscript; their comments were of great value.

BOTTOM CAMERA STATIONS

Camera stations were occupied at regular intervals between 17 April 1983 (day 117) and 3 May 1983 (day 133). The UMEL camera was used on the frame designed by N. Fenerty (Bedford Institute of Oceanography, Photographic Laboratory) for use on ice station AIDJAX. The camera frame used in this program was originally designed to be lowered through 40cm diameter hydroholes. The frame, which is about 2m in length, was deemed not appropriate to the hydroholes cut at CESAR (a more conventional frame, such as those used at sea, may be easier to handle and should be considered for future ice camps). A trip weight, which fired the camera, was suspended 2m below the frame. The resulting field of view of photographs was approximately 1 × 2m (lens focal length: 35mm). Table 4.1 shows the camera stations occupied in association with the latitude, longitude, water depth, and general bottom conditions. Both black-and-white and colour slides were used in the program. A total of 605 useable seabed photographs were taken during 14 lowerings. No results were obtained from stations 1, 6 and 7.

The positions of the camera lowerings relative to regional bathymetry are shown in Figure 4.1. The lowerings cover a range in depths from 1160 to 1690m. The shoalest point is situated on the crest of an eastward-plunging sub-ridge in the northern Alpha Ridge chain. The deepest lowering was situated in the trough (Alpha Ridge graben) south of the northern Alpha Ridge crest.

Table 4.1. CESAR bottom camera stations

Station no.	Film type	No. of exposures	Day/time (GMT)	Latitude (°N)	Longitude (°E)	Water depth (m)	Description
1	B & W	—	117, 2200	85° 53' 0.5"	251° 15' 39.1"	—	Flash did not work.
2	B & W	63	118, 2230	85° 52' 58.4"	251° 18' 40.6"	1500	Flocculated silts with rounded dropstones.
3	B & W	50	119, 2330	85° 52' 49.4"	251° 20' 53.0"	1530	Flocculated silts with rounded dropstones.
4	B & W	80	120, 1830	85° 52' 45.4"	251° 22' 11.8"	1520	Flocculated silts with rounded dropstones.
5	Colour	40	121, 2130	85° 52' 24.9"	251° 21' 41.0"	1490	Gravelly, silts with dropstones.
6	—	—	—	—	—	—	—
7	—	—	—	—	—	—	—
8	B & W	90	125, 2200	85° 49' 49.4"	250° 52' 37.0"	1630	Gravelly, silts with dropstones.
9	B & W	83	127, 1700	85° 49' 32.2"	250° 45' 12.8"	1680	Gravelly, silts with dropstones.
10	Colour	30	129, 1530	85° 49' 29.4"	250° 45' 35.3"	1690	Scouring around dropstones.
11	B & W	50	130, 1530	85° 49' 34.2"	250° 50' 30.9"	1630	Gravelly silt with dropstones (scour around dropstone).
12	B & W	10	131, 2400	85° 50' 8.3"	251° 0' 29.4"	1282	Gravelly silt with dropstones (scour around dropstone).
13	B & W	13	132, 1900	85° 51' 4.3"	251° 14' 9.6"	1195	Gravelly silt with dropstones (scour around dropstone).
14	B & W	96	133, 0130	85° 51' 31.5"	251° 21' 55.9"	1222–1160	V. gravelly silt with dropstones (scouring visible abundant bioturbation and starved ripples).
		605					

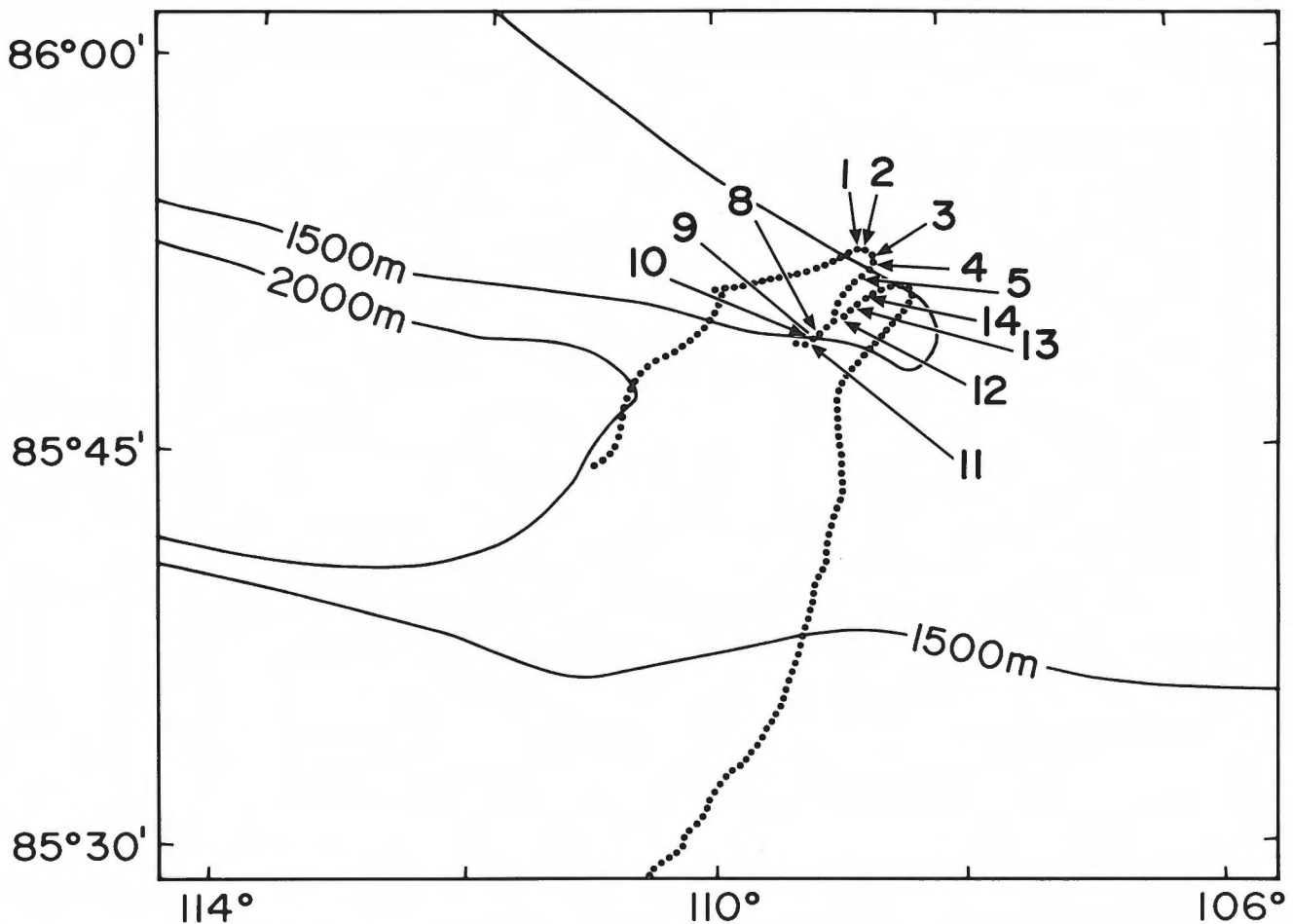


Figure 4.1 Position of CESAR bottom camera stations.

Lowerings 2 to 9 (Plate 4.1) all show similar seabed character. The sediment is bimodal in constituent grain sizes and reflects two modes of origin. The fine matrix of clayey material, which is easily suspended, is thought to be derived principally from the erosion of bedrock which outcrops locally.

The second mode is a coarser fraction, which shows a gradation in size from fine sand to boulders. The gravel size material occurs with random distribution and, where observed, was restricted almost exclusively to the surface (drag marks of the trip weight show an exposed, well sorted fine sediment beneath the surface veneer). These coarser sediments are considered to be ice-rafted and subsequently released from melting multiyear ice. No postdepositional transport of either the finer or coarser fraction was evident. The gravelly "dropstones" show a variety of shapes and sizes consistent with the findings of Schwarzacher and Hunkins (1965). However, many are subrounded to rounded suggesting previous reworking in a fluvial or beach environment. Schwarzacher and Hunkins (1965) and Crombie (1960), by contrast, suggested the source of the dropstones is glacial till.

The gravel fraction shows no evidence of burial, as the clasts always occurred with an Fe/Mn coating. It is thus inferred that the deposition rate of fine grained sediment is

extremely slow. This is consistent with the previous studies of Clark et al. (1980).

The impact marks of the 5kg trip weight was never greater than approximately 1cm (depth inferred from shadow length). The inference thus made is that the sediment is well compacted, suggesting an extremely low deposition rate.

Bottom currents have been interpreted from the bottom photographs. They are based on sediment drift rates of the trip weight impact plume observed from frame to frame. The drift rates are 1-2cm s⁻¹ to the west at stations #2, 5, and 8, and 1-2cm s⁻¹ to the south at station #4. Hunkins et al. (1960) observed flows of less than 1cm s⁻¹ from the Alpha station, while Hall (1979) working in the same region, reported a near bed flow of 1cm s⁻¹. Hunkins et al. (1969), in a similar fashion, measured bottom currents of 4-6cm s⁻¹.

Successive trip weight impact prints were seen from image to image of the bottom photographs. The distance between impacts shows an ice drift rate of approximately 20cm min⁻¹ or less. On the short term it appears that the ice moves in bursts of motion, separated by short intervals of no motion. Furthermore, the direction of ice drift appears to fluctuate $\pm 30^\circ$ about the net drift direction. It should be noted, however, that some of the above observations may be

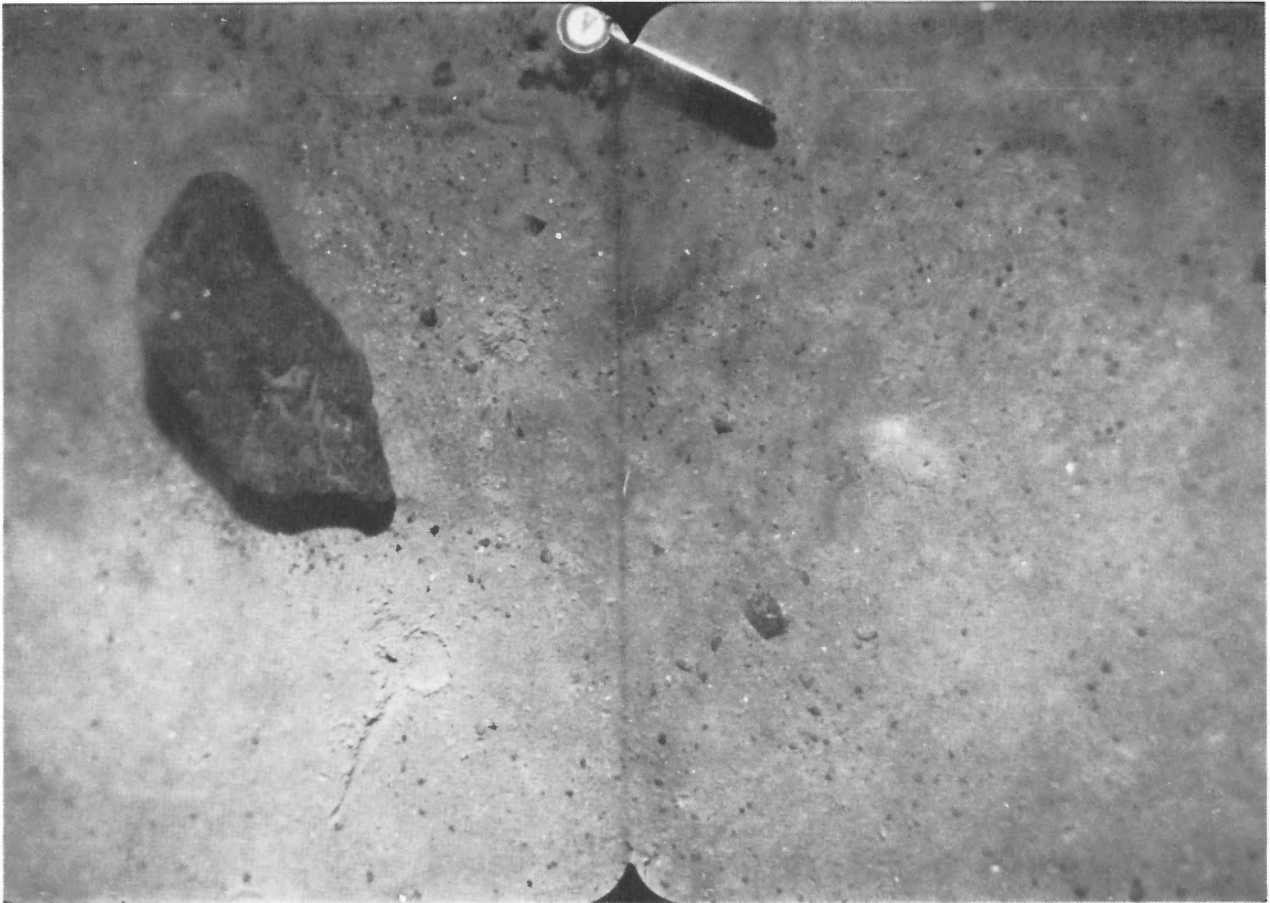


Plate 4.1

Seabed at site 9, 1680m water depth, showing poorly sorted, randomly distributed coarse material on a well compacted surface of well sorted fine sediment. Field of view 1×2 m.

the result of variations in the wire angle on which the camera is suspended.

All photographs from stations #2 to 10 show some evidence of bioturbation. The surface is covered with a film of what appears to be organic debris. Bioturbation is greatest in the deepest stations #8, 9, and 10. Star-shaped imprints are common. These imprints are approximately 15cm in diameter and usually have 6 radial arms. Gravel fragments, considered to have been derived from ice rafting, litter the seabed in a random fashion (Plate 4.1).

The results from stations #9 to 14 show a gradual increase in the gravel fraction and decrease in the finer mode as the bathymetry shoals from 1680 to 1160m. Station #11 shows a gravel cover of 30% (by area) and an irregular distribution of material. Haloes around the larger fragments are seen, but are considered biogenic in view of the abundant trail marks. Station #12, in 1282m of water, shows a gravel cover of 50%. No evidence of any currents were observed. Station #13, in 1195m of water, shows a 70% gravel cover. The increase in gravel is paralleled by a decrease in evidence of bioturbation. Crombie (1960) observed a coarsening of bottom sediments over the Alpha cordillera, but offered no explanation of the processes responsible for the trend.

Station #14, the shoalest station (1160m water depth), shows 70 to 100% gravel cover (Plate 4.2). Only a small sediment plume was given off by the impact of the trip weight at the seabed, indicating a prior winnowing of the ubiquitously deposited fine grained material. The trip weight imprint is scarcely visible, showing that the seabed is relatively hard. The gravel is weakly aligned parallel to the current observed from adjacent stations and shows a motion to the southwest. Scour marks around cobbles show typical current scour patterns with asymmetric tails which are oriented east and west. Such marks are considered not to be associated with a biogenic origin.

Starved ripples were observed at station #14 (Plate 4.3). The ripple crests are interpreted to be oriented 90° to the flow direction. These ripples appear to be composed of sand-size Fe/Mg rich micronodules. The crests of the ripples are rounded and undulate in plan view. Such features are usually formed by near bed unidirectional flows of about 20cm s^{-1} (Middleton and Southard, 1978). No ripple marks are present in the bottom photographs described by Cromie (1960) and Schwarzacher and Hunkins (1965). Therefore their occurrence is unusual and the distribution of these features is considered to be limited. This is probably due to the paucity

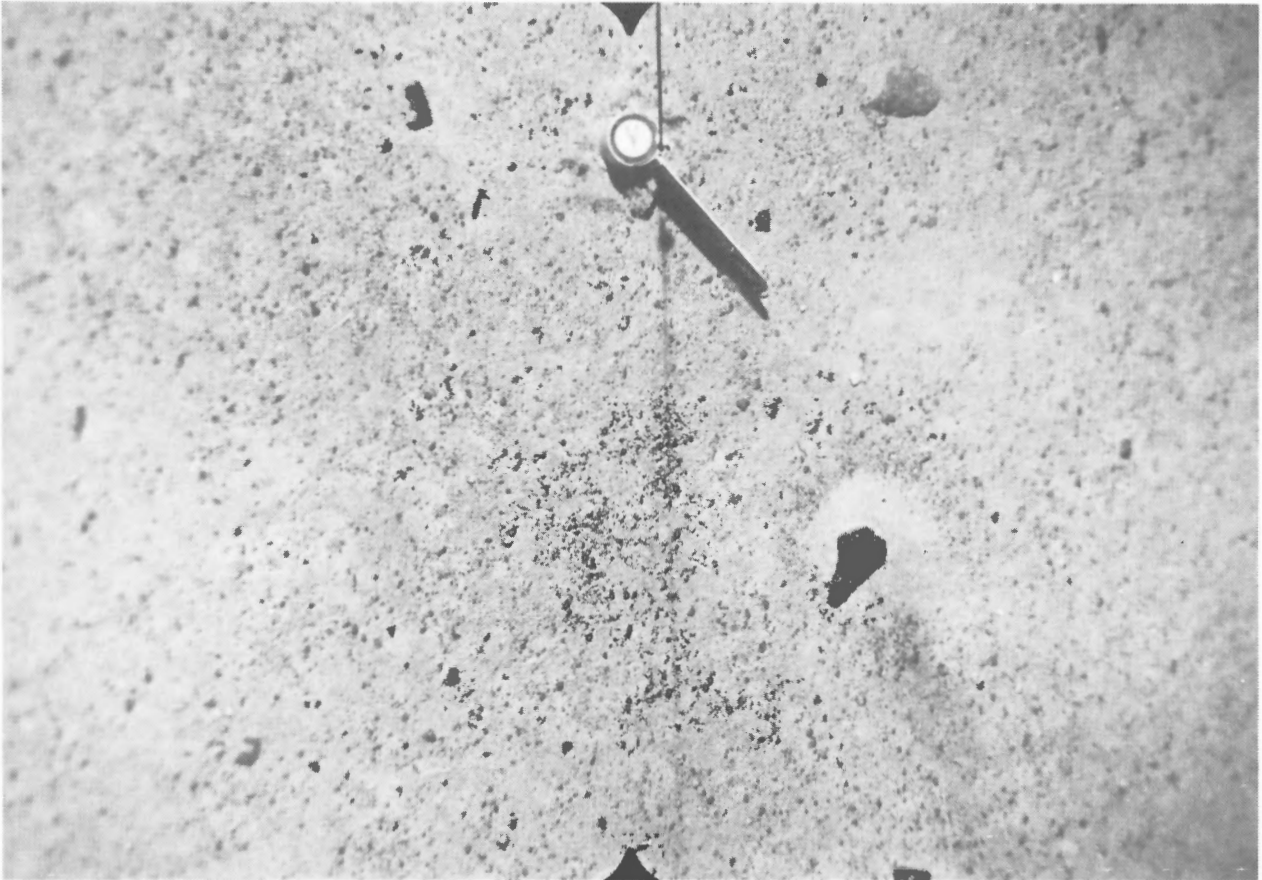


Plate 4.2

The seabed at site 14 (1160m water depth) showing a dense gravel cover comprising a relatively hard seabed. Scour current patterns around cobbles show east-west orientation. Field of view 1×2 m.

Bedrock is thought to outcrop at the surface at station #10 (see Fig. 4.2). Analysis of this material recovered in dredges show it to be well weathered basalt (Van Waggoner and Robinson, 1985). The outcrop shows evidence of in situ fracturing and mechanical breakdown. The breakdown of the exposed bedrock surface appears to be providing clay material to the adjacent deeper troughs. Herman (1974), who classified bottom sediment into six types on the basis of source and mode of transport, does not consider seabed weathering of bedrock. Yet in the region pertaining to this study it appears to be a dominating supplier of fine grained material.

DISCUSSION

The change in bed texture from pelagic deposition in 1600m of water, to a winnowed, hard gravelly bed in 1100m of water is difficult to explain. It is not associated with surface wave activity (due to depth of water and ice cover). Moreover, there was no obvious water column stratification or vertical variation in water mass. Thus sedimentation is likely related

to the winnowing of the sub-ridge crest by the infrequent passage of near-bottom storm driven currents. The troughs between the sub-ridges appear to be regions of accumulation of ponded sediment. Such sedimentation patterns are not always expected in the deep sea, where conformable bedding, as defined by Piper et al. (1983) is often more appropriate. The relative sheltering of the troughs suggests storm currents moving transverse to the ridge system, i.e. possibly in the north-south quadrants.

Clark et al. (1980) plotted the distribution of coarse sediment (greater than 64 microns) in the bottom sediments over the Alpha cordillera. They show the highest proportions (approximately 25%) to occur on the south flank of the ridge. This is the site of bedrock outcrop and perhaps argues for a significant supply of seabed material by weathering and dispersal of local material.

BOTTOM DREDGING

Dredging was attempted at 18 sites from 10-20 April 1983 (day 110-120) and in water depths ranging from 1040-2050m. A list synthesizing the dredging activities is given in Table 4.2. The positions of the dredge sites in relation to the camp drift is shown in Figure 4.2.

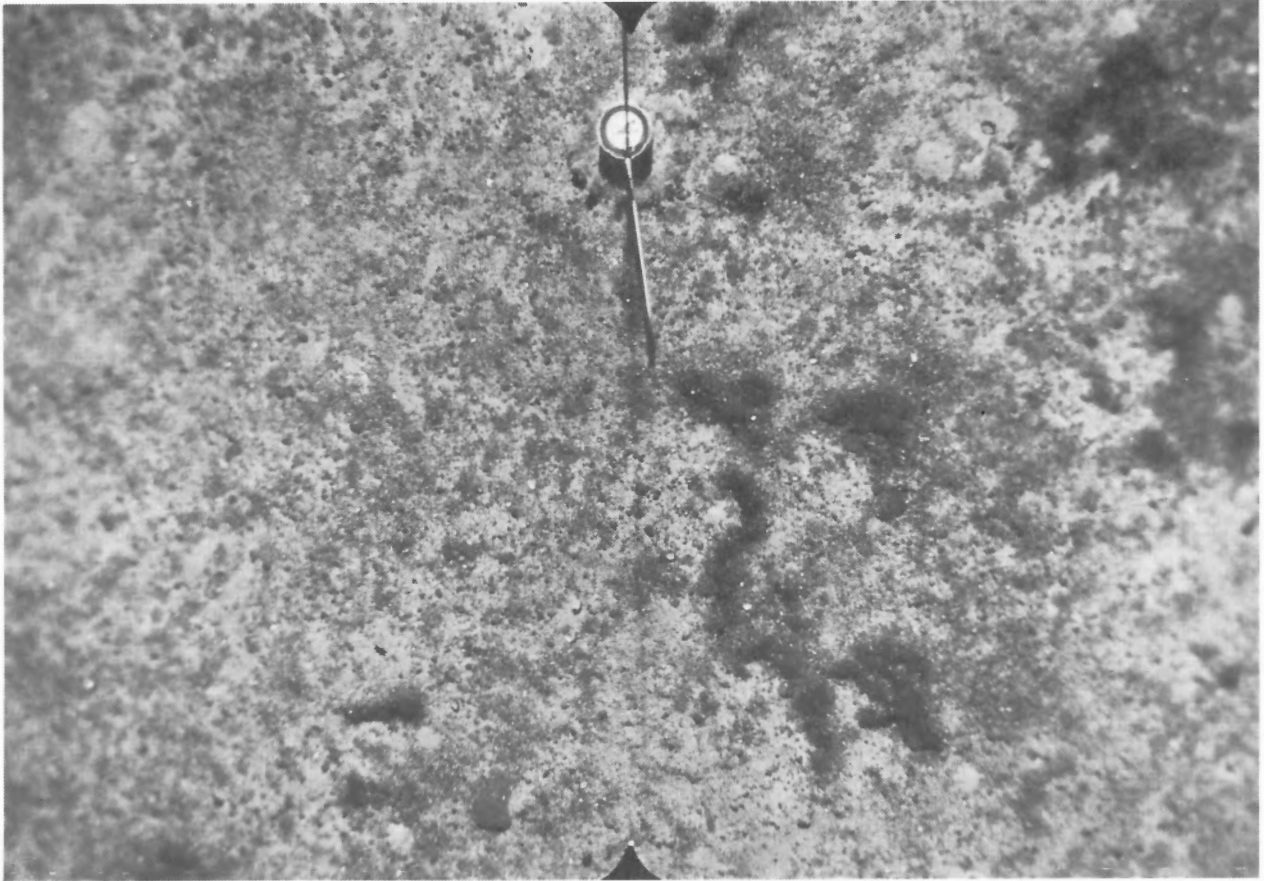


Plate 4.3

Seabed at site 14, 1160m water depth, showing undulating ripples with rounded crests, formed in sand. Field of view 1 × 2m.

Table 4.2. CESAR bottom dredge stations

Station no.	Day – Time (Down)	Latitude (°N)	Longitude (°E)	Water depth (m)	Time up (GMT)	Description
D1	110, 1200	85° 45' 38.9"	249° 10' 46.5"	1850		No recovery – one dropstone.
D2	110, 2400	85° 45' 5.9"	249° 3' 13.6"	1890	0800	No recovery.
D3	112, 2100	85° 45' 22.6"	249° 7' 37.6"	1850	0110	No recovery.
D4	113, 0140	85° 45' 36.8"	249° 8' 23.6"	1852	0700	Rock samples + mud.
D5	113, 1540	85° 47' 5.4"	249° 13' 27.4"	2050	2130	Rock samples + mud.
D6	113, 2230	85° 48' 1.1"	249° 17' 27.5"	2000	0530	No recovery.
D7	114, 0550	85° 49' 4.0"	249° 32' 23.3"	1984	1630	Trace of fine material.
D8	114, 1730	85° 50' 0.7"	249° 51' 6.0"	1850	0016	Dropstones.
D9	115, 0030	85° 50' 24.7"	249° 55' 45.1"	1650	0520	No recovery – high tension on cable.
D10	115, 0540	85° 51' 7.4"	250° 1' 30.5"	1100	1620	Bedrock & dropstones.
D11	115, 1630	85° 51' 52.9"	250° 15' 20.3"	1040	2300	No recovery.
D12	115, 2330	85° 52' 11.3"	250° 38' 10.2"	1200	0400	One dropstone.
D13	116, 0430	85° 52' 18.8"	250° 46' 21.8"	1380	1540	Muddy sediment with one dropstone.
D14	116, 1600	85° 52' 49.6"	251° 6' 8.5"	1450	2330	No drift of ice.
D15	117, 0440	85° 53' 8.1"	251° 12' 39.7"	1500	1650	No drift of ice-mud on bucket.
D16	118, 0120	85° 53' 0.6"	251° 15' 36.9"	1550	2109	No recovery.
D17	119, 0600	85° 52' 58.9"	251° 18' 54.4"	1550	2012	No recovery.
D18	120, 0630	85° 52' 44.7"	251° 21' 49.8"	1500	1639	No recovery.

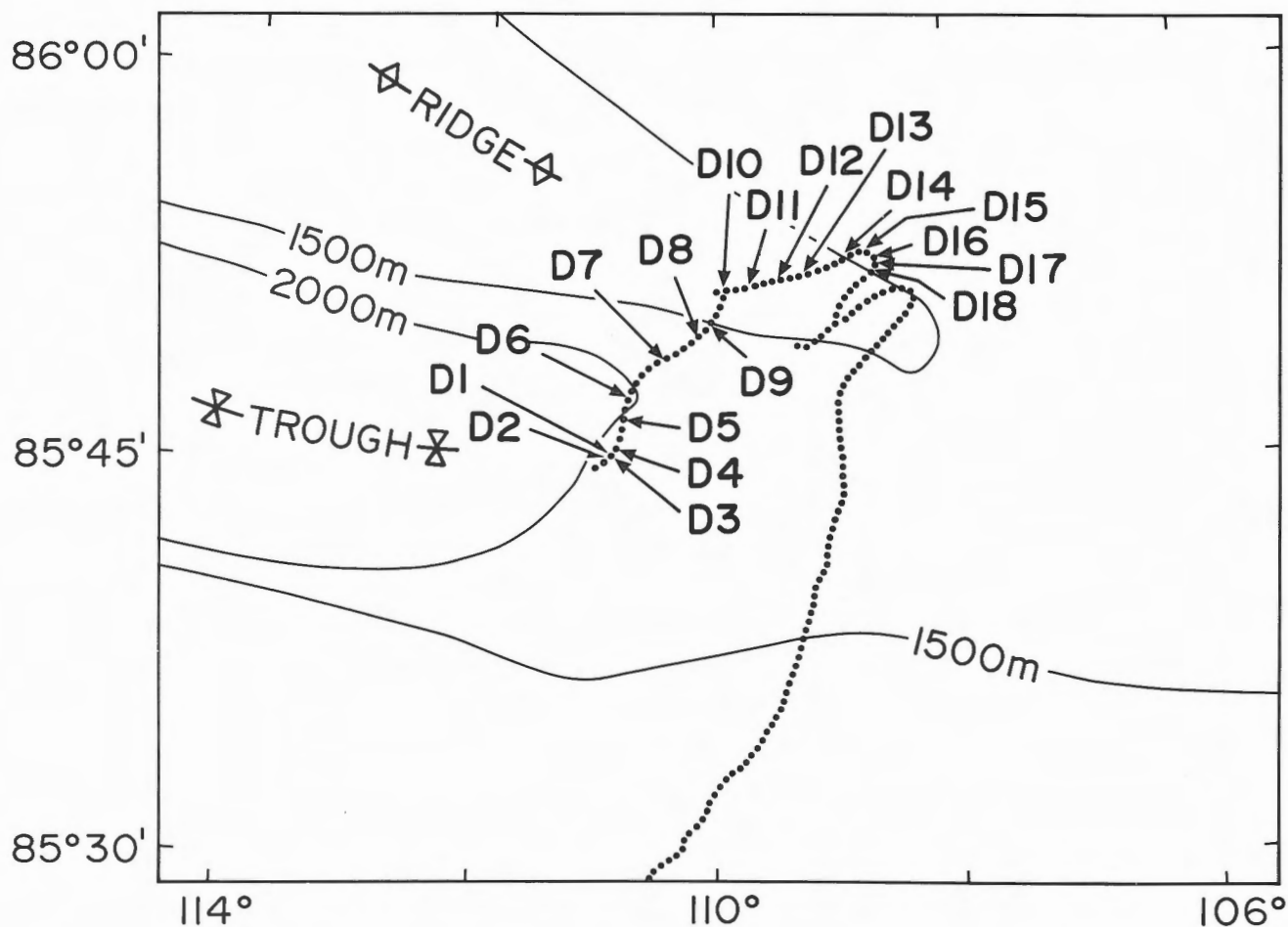


Figure 4.2 Position of CESAR bottom dredge samples.

The recovery of bottom material was variable due to the low drift rate of the ice and due to variations in bottom roughness. Material dredged from the deeper trough (D1-D7) was composed of a fine grained plastic ooze which was recovered interspersed with granule- and cobble-sized fragments. In general the size frequency histogram of bottom sediments follows closely type IV sediments recovered by Clark et al. (1980) over the Alpha cordillera (see Fig. 4.4 A to I).

The sand-sized sediment (greater than $63\mu\text{m}$) is typically bimodal. The finer mode is composed of angular grains of clear and yellow stained quartz (d_{50} : $100\text{-}200\mu\text{m}$) which comprise approximately 40% of the mode, and biogenic material which comprises the remainder. The biogenic material is composed predominantly of globigerinids (d_{50} : $200\mu\text{m}$), benthic foraminifera (d_{50} : $800\mu\text{m}$) and sponge spicules (Plate 4.4, Table 4.3). The allogenic material of the finer mode is well sorted, reflecting hydraulic transport. The quartz is associated with a subpopulation of semiprecious metals and mafics which have a modal size of $100\mu\text{m}$. These fragments are considered to be hydraulically equivalent to the angular siliceous material. The population, by virtue of its composition, is considered to be derived by ice rafting. A

discussion of the original sources of this ice-rafted material will be given later.

The coarser mode is poorly sorted and shows a gradation in size from $800\mu\text{m}$ to 0.3m . This mode is composed predominantly of well rounded quartz and lithic fragments which are partially Fe/Mn stained. It comprises very little biogenic debris. This mode is considered to be derived by the process of ice rafting. The material entrapped in the pack-ice is released during summer melting and is dropped in situ. The distribution of this material is therefore not controlled by bathymetry. The Fe/Mn coating (usually restricted to one side) shows no postdepositional transport and indicates extremely slow sedimentation rates.

Four dropstones were recovered in dredge D4 and five in dredge D5. Macroscopic analysis and acid testing suggest that they are predominantly composed of dolomite, with minor amounts of calcite. One of the fragments was composed of yellow stained gypsum (Table 4.4). The majority of these hand specimens are very well rounded and lack fracturing or pitting typical of a glacial origin. It is thought that they were incorporated into the ice after either a period of fluvial transport to the coast, or by reworking in a beach zone.

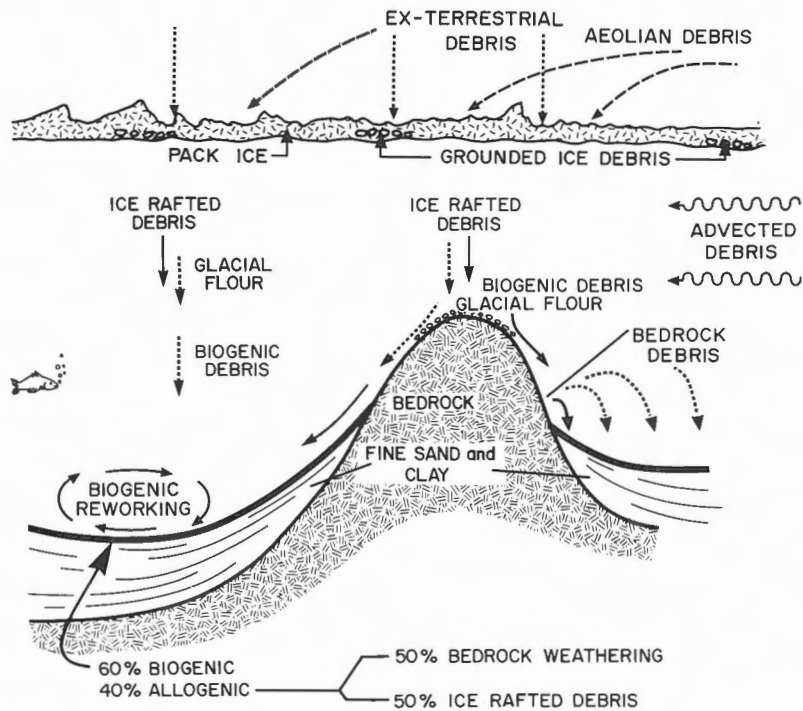


Figure 4.3 Sketch depicting the main sources of sediment supplied to the seabed of the northern Alpha Ridge crest and graben.

Dropstones recovered by Crombie (1960) from the same general region were reported to be principally composed of limestone. Schwarzacher and Hunkins (1965) described both angular and well-rounded dropstones from 8 dredges carried out to the west of the Alpha Ridge. These samples were predominantly sandstone and shale with 20 to 50% of fragments composed of dolomite. We recovered, by contrast, only one sample composed of sandstone/shale.

Dolomite and limestone is abundant on eastern Bathurst Island (Disappointment Bay Formation) and on the north coast of Ellesmere Island (Wilderness Carbonates of Ordovician age). These formations are considered to be the sources of the dropstones. The similarity in clast compositions is remarkable, and suggests a longstanding constant drift pattern of the polar ice pack.

Six dropstones recovered in dredge D8 are similar in composition (dolomite) to those recovered from the deeper trough to the south (D5). Two of the samples were composed of carbonaceous dolomite perhaps associated with the Ellesmere Island Wilderness Carbonates.

The most significant recovery was made during dredge D10, which recovered what we consider to be fragments of bedrock interspersed with 7 ice-rafted dropstones. The bedrock material showed "fresh" surfaces of well weathered basalt and an upper surface of manganese encrusted serpulid tubes (G. Gross, personal communication, 1985). The bedrock samples were recovered from the steeply dipping south flank of the northern Alpha Ridge crest (see Table 4.2) and were associated with extremely high wire tension, chattering of the dredge bucket and an acoustically "hard" seabed. Mineralogical and chemical analysis of the bedrock sample is given by Van Wagoner and Robinson (1985). A cursory binocular microscope examination of the sample suggests it is

well weathered pyroclastic basalt. The dominant constituent is well weathered feldspar which has become broken down to friable pseudomorphs. The weathering of the feldspar and its subsequent dispersal is considered to produce the finer (silt/clay and fine sand) material of the local surficial sediments.

The northern Alpha Ridge crest was sampled during dredges D11, D12, and D13. Sand or fines (silt/clay) were recovered only in dredge D13. Similar sediment characteristics to those in dredge samples D4 and D5 were observed, except that much less clayey material and a higher percentage of iron-stained quartz was present.

One dropstone was recovered in each of dredges D12 and D13. These samples were composed of siltstone and dolomite respectively. Both specimens were well rounded.

The interpretation of the regional pattern of sedimentation is depicted in Figure 4.3 and the grain size statistics are given in Table 4.5. Ice-rafted debris is deposited over the entire seabed irrespective of topography. This material is principally derived from the Ellesmere Island coast (or Axel Heiburg and North Greenland as suggested by Schwarzacher and Hunkins, 1965) and is composed of an entire spectrum of sizes (up to 0.3m in diameter).

Biogenic debris in the form of globigerinids, foraminifera, radiolaria, sponge spicules and ostracods are deposited pelagically and appear to collect preferentially in the deeper areas. This source comprises approximately 40% of the sand size fraction on the ridge crest and 60% in the trough centre.

The inorganic silt and clay fractions are interpreted to be derived from three major sources: (1) breakdown of bedrock outcropping on the flanks of the northern Alpha Ridge; (2) ice rafting; and to a lesser extent (3) advection in the water column.

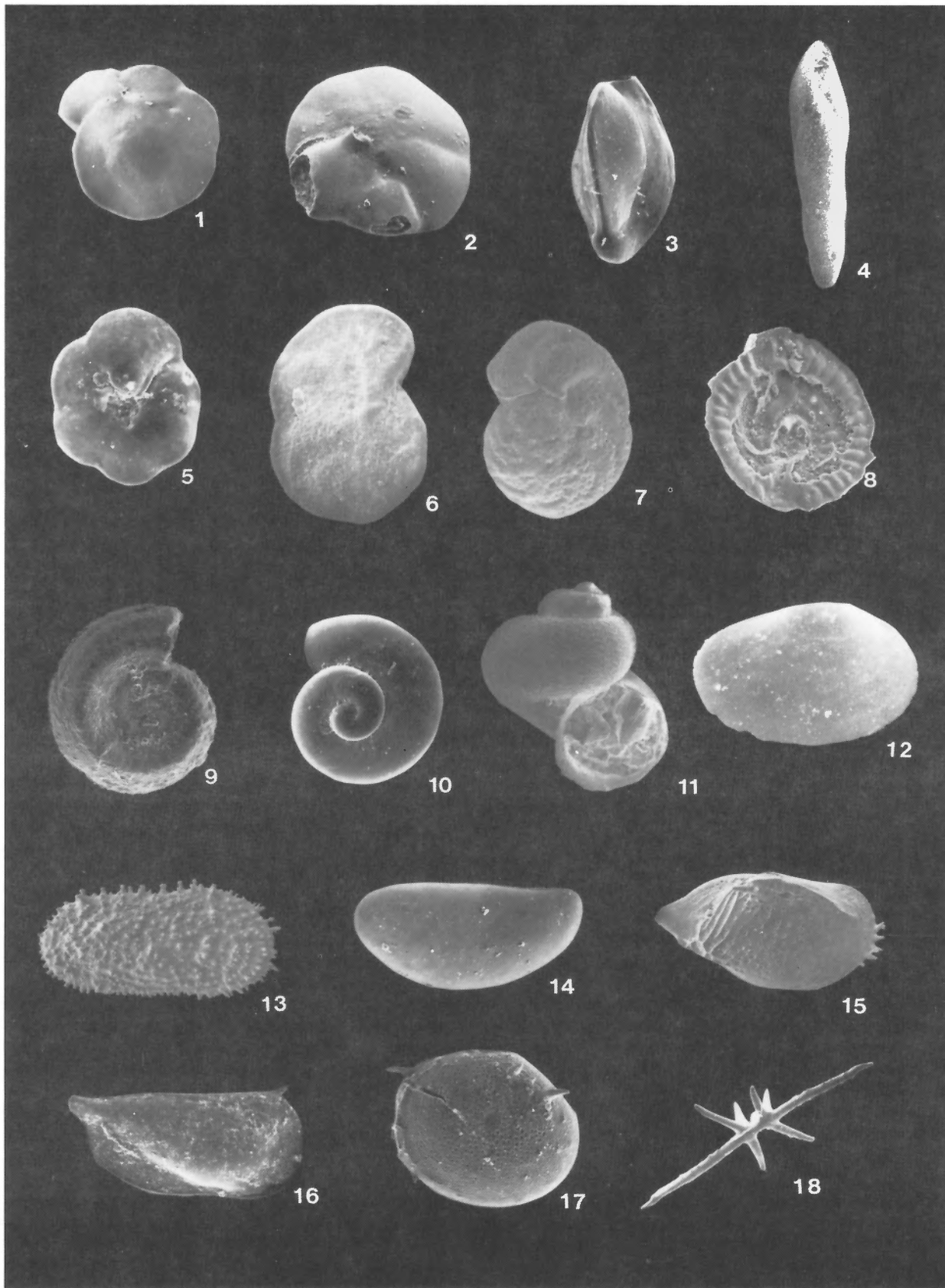


Plate 4.4

SEM photographs of benthic foraminifera, molluscs, ostracods and sponge fragments from CESAR dredge samples.

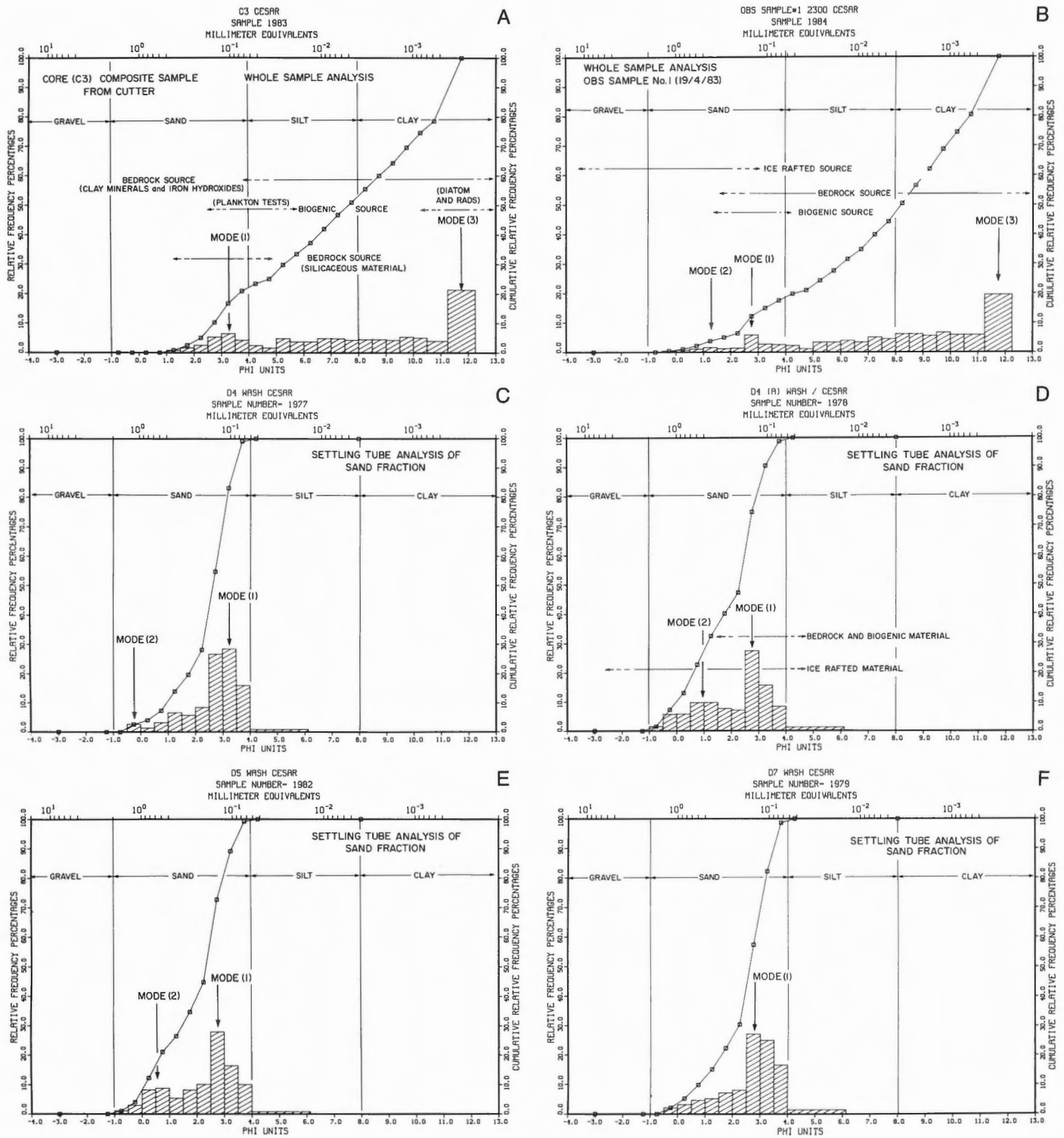


Figure 4.4 Seabed sediment size analysis of eight samples collected during the dredging coring program. An interpretation of the size class histogram modes is also presented.

- A Core cutter sample from core C3.
- B Surface sample from OBS station (19/4/84).
- C Settling tube analysis of coarse fraction (>63µm) from dredge D4.
- D Duplicate analysis of coarse fraction (>63µm) from dredge D4.
- E Settling tube analysis of coarse fraction (>63µm) from dredge D5.
- F Settling tube analysis of coarse fraction (>63µm) from dredge D7.

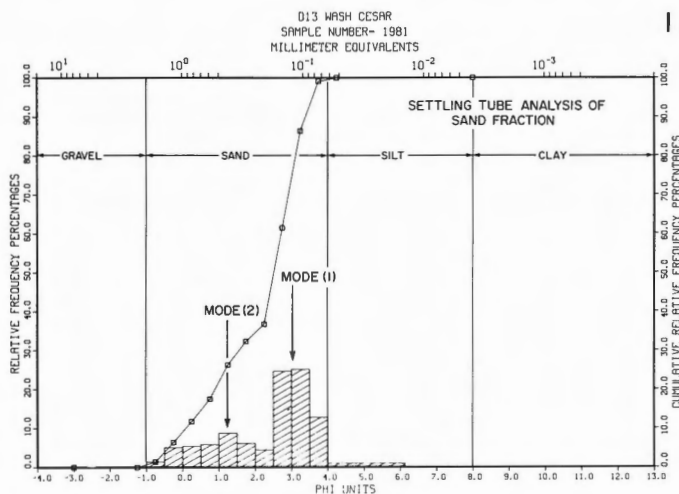
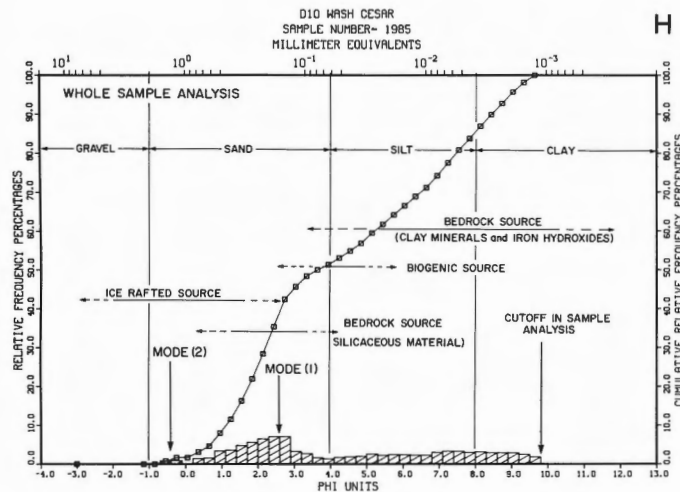
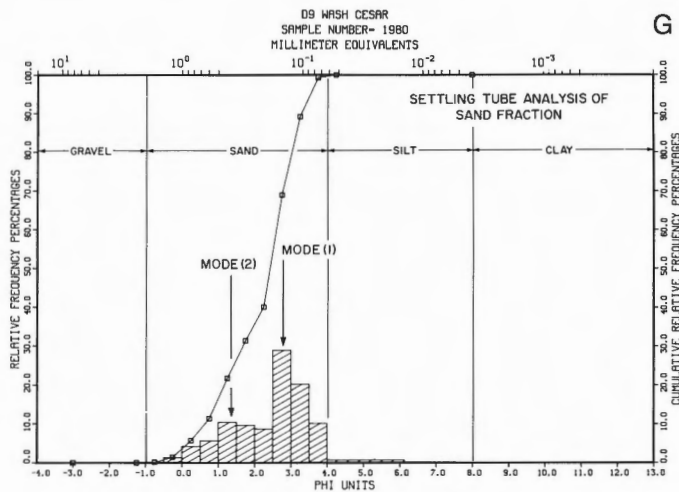


Figure 4.4 (cont'd)

- G Settling tube analysis of coarse fraction (>63µm) from dredge D9.
- H Whole samples analysis of material from dredge D10.
- I Settling tube analysis of coarse fraction (>63µm) from dredge D13.

Once deposited, the seabed appears to consolidate to form a semi-indurated sediment presumably by the process of gravity settling with time. The resulting cohesive material (assuming a vane shear strength of 4 KPa which is considered representative) would erode at a near bed current of approximately 1.5m. s⁻¹ (Kamphuis and Hall, 1983). Therefore, postdepositional erosion is unlikely to have taken place. Well preserved sponge spicules also attest to a lack of erosion.

SUSPENDED PARTICULATE MATTER (SPM)

The concentrations of suspended particulate matter were determined at regular intervals throughout the water column during the period, 4-6 April 1983. Up to 12 L of seawater, collected using Niskin sample bottles, was filtered through 0.45µm NuclePore^R filters. Due to the extremely low concentrations of SPM and the uncertainty associated with the results, the program was repeated by filtering 100 L of seawater collected using Niskin samplers. The results are given in Table 4.6.

The depth averaged suspended sediment concentration (SSC) of the water column was 0.08mg. L⁻¹ (± 0.07). The maximum recorded value was 0.24mg. L⁻¹, though much of

this (20 to 50%) can be ascribed to residual salts precipitated on the filter pad during filtering. Concentrations were generally higher than anticipated and showed a general decrease from the surface to the seabed. The concentration of particulate matter in the ice samples (taken from 3 different sites away from main camp) were remarkably consistent at 0.11mg. L⁻¹ (± 0.05) and were significantly higher than concentrations in the underlying water mass.

A detailed analysis of the particulate matter has been made on samples from the ice, the water column and seabed. This involved grain size analysis of the disaggregated material, a visual analysis of particles using a Cambridge[®] Stereo Scan 180 scanning electron microscope, and an elemental analysis of particles using the EG & G EEDS II EDAX elemental analyzer fitted to the SEM. Results of the microscopic analysis are given in Table 4.7. The synthesis includes an analysis of an ice sample and the breakdown products from the dredged bedrock sample.

The ice sample exhibited particles ranging from 3 to 100µm in diameter. A variety of these particles are illustrated in Plates 4.5 and 4.6. In general terms, two major sources of material were detected. The major source is considered to be terrestrial, derived by eolian transport. Angular unweathered

Table 4.3. Taxonomic composition of biogenic material in coarse fraction (> 63 µm) of CESAR dredge samples D4, D5, D7, D9, D13 and core sample C13

Group	Species Fauna	Abundance
Foraminifera – Planktonic	<i>Neogloboquadrina pachyderma</i>	Abundant
– Benthic:		
Calcareous –	<i>Dentalina frobisherensis</i>	Occasional
	<i>Eponides tumidulus</i>	Occasional
	<i>Oridorsalis tener</i>	Occasional
	<i>Patellina corrugata</i>	Occasional
	<i>Planulina wuellerstorfi</i>	Common
	<i>Pyrgo</i> Sp.	Occasional
	<i>Quinqueloculina elongata</i>	Occasional
	<i>Quinqueloculina vulgaris</i>	Common
	<i>Robertinoides charlottensis</i>	Occasional
	<i>Stetsonia</i> Sp.	Occasional
	<i>Triloculina carinata</i>	Occasional
	<i>Virgulina</i> Sp.	Occasional
– Benthic arenaceous –	<i>Trochammina nitida</i>	Very rare
Molluscs	Gastropod	Occasional
	Pelecypod	Occasional
	Serpulid worm	Occasional
	<i>Spiratella helicina</i>	Common
Ostracods	<i>Echinocythere</i> Sp.	Frequent
Otoliths	Ca. 12 unknown Sp.	Frequent
	Unknown	Very rare
Radiolaria	None	Absent
Sponge	Few Spp.	
Occasional		
	<i>Flora</i>	
Diatoms	<i>Coscinodiscus</i> Sp.	Rare
Dino/layellate calcispheres	None	Absent

Table 4.4. Identification based on reflected light microscopic examination, acid testing (HCl) and hardness.

Dredge No. – Sample No.	Composition	Shape
D4-1	Dolomite	Well rounded
-2	Dolomite	Subangular
-3	Limestone/dolomite	Subrounded
-4	Dolomite	Subrounded
D5-1	Dolomite	Angular
-2	Dolomite	Rounded
-3	Dolomite	Rounded
-4	Red-stained dolomite	Rounded
-5	Carbonaceous dolomite	Rounded
-6	Carbonaceous dolomite	Rounded
D8-1	Dolomite	Subrounded
-2	Dolomite	Rounded
-3	Dolomite	Subangular
-4	Dolomite	Rounded
-5	Carbonaceous dolomite	Rounded
-6	Carbonaceous dolomite	Rounded
D10-1	Dolomite/limestone	Angular
-2	Dolomite/limestone	Rounded
-3	Limestone	Rounded
-4	Limestone	Subrounded
-5	Limestone	Angular
-6	Greywacke	Subrounded
-7	Vuggy volcanic	Rounded
D12-1	Siltstone	Well rounded
D13-1	Dolomite	Well rounded

Table 4.5. Grain size analysis of bottom sediment samples.

Sample #	Gravel	Sand	Percentage		Mean (Phi)	Sorting (Phi)	Skew
			Silt	Clay			
OBS # 1 (19/4/83)	0	17.5	26.8	55.7	7.8	3.2	-0.6
Core # 3 (Barrel)	0	21.0	30.0	49.0	7.6	3/2	-0.2
D4(A) (>53µm)	0	98.8	1.2	0	2.1	1.2	-0.5
D4 (>53µm)	0	99.1	0.9	0	2.7	1.0	-1.2
D5 (>53µm)	0	99.2	0.8	0	2.2	1.2	-0.6
D7 (>53µm)	0	98.6	1.4	0	2.6	1.0	-1.0
D9 (>53µm)	0	99.3	0.7	0	2.4	1.0	-0.7
D10	0	50.9	32.9	16.2	4.5	2.8	0.3
D13 (>53µm)	0	99.1	0.9	0	2.3	1.2	-0.8

fragments of mica (Plate 4.5E), orthoclase (Plate 4.5B) and quartz (Plate 4.5A) are dominant components of this source. Many of these fragments show sharp "feather" edges (Plate 4.5B), and conchoidal fracturing (Plate 4.6A) indicating a lack of abrasion. Similar fragments have been documented by Clark et al. (1980) from various horizons within cores collected throughout the Arctic Ocean. Wood fragments (Plate 4.5C) and pollen grains (Plate 4.6F) were also present. The composition and crystalline nature of the eolian material suggests ablation of granitic rocks. The Paleozoic gneisses, schists and granites from north and east Ellesmere Island may well be the source.

The marine component of the ice trapped sediment includes diatom tests (Plate 4.5D), iron rich rosettes and clay floccules (Plate 4.6D). The floccules are bound by undifferentiated organic matter and comprise material finer than 30µm. Fine silt and clay size particles appear to be entirely marine. By contrast to previous studies, no ice-rafted silt or clay particles were unequivocally identified. One pure iron spherule, interpreted to be a micro-meteorite, was observed in the ice sample. The specimen is shown in Plate 4.6B and 4.6C.

The marine particulate material was analyzed from depths of 25m (Plate 4.7), 350m (Plate 4.8A, 4.8B), 1000m (Plate 4.8C), and 1330m (Plate 4.8D to 4.8F). Particles ranged in size up to 150µm. Material was in general bimodal with particles of approximately 30-50µm and 1-5µm dominating the size spectrum.

The majority of particles fall within either of two classes; iron-rich to pure iron agglomerates or silica- and aluminum-rich clay mineral floccules. The iron-rich floccules occur at all depths and at all sizes. They are interpreted to be derived from the iron-rich pyroclastic basalt which outcrops on the south flank of the Alpha Ridge subcrest.

The clay floccules shows variations in preservation of plate structure, composition and size. The floccules are principally composed of smectite (see Table 4.7) and often include diatom fragments. They also show traces of titanium, chromium, lead, zinc, manganese and magnesium. The dominance of silica, aluminium and potassium suggests that the material is a well weathered feldspar (possibly microcline). The most probable source of this material is the local bedrock as previously discussed.

A predominance of mica flakes was observed in the sample taken from a depth of 1000m. Although the significance of this "mica peak" is not known, the advection of material from the North Atlantic may well be the source. There appears to be no other segregation of particles either on the basis of size or composition. No evidence was found to support the hypothesis of Clark et al. (1980), that mid-depth flow is an important mechanism for the sorting of sediment deposited at the seabed.

An analysis was made of the weathered bedrock material from dredge D10 (Plates 4.9) to compare results to those derived from the suspended particulate matter (SPM) of the

Table 4.6. The results of the analysis of the concentrations in suspended particulate matter from ice and seawater samples. The analysis error, based on sample variability, is approximately $\pm 0.07 \text{ mg L}^{-1}$ at the 68% confidence level. A sample volume of 100 L was filtered in all cases.

Sample #	Depth (m)	SSC (mg L ⁻¹)	SEM. #
5412	ice	0.10	84-09
5351	ice	—	
5379	ice	0.11	—
5302	2.7m	0.11	
5353	75m	—	
5283	100m	—	
5408	150m	0.08	
5411	150m	0.16	
5285	200m	0.04	
5419	250m	0.21	
5418	250m	0.01	
5402	300m	0.24	
5404	400m	0.05	
5406	350m	0.04	84-10
5369	500m	0.01	
5416	600m	0.01	
5360	750m	—	
5414	875m	0.16	
5323	1000m	0.08	
5321	1100m	—	
5306	1200m	0.03	
5337	1300m	0.19	
5304	1300m	0.02	
5332	1310m	0.01	
5358	1330m	—	
5358	1330m	—	
5435	1500m	0.08	
5427	1700m	0.03	
5433	1740m	0.12	
		SSC = 0.07	

Table 4.7 S.E.M. analysis of particulate matter from the ice pack, the water column and seabed from the CESAR site.

Sample #	Grain diam. μm	Elements											Micrograph		Interpretation		
		Si	Al	Fe	K	Mg	Mn	Ti	Na	Ca	Cu	Cr	No.	(Mag.)			
F.229 (Ice) 84-09	100	M	M	T	M									09-5		Ortho-felspar (unweathered angular)	
	100	I		M										09-1-4	(1020)	Ferro-silicate (conc. fract.)	
	100													09-6	(410)	Wood fibre	
	30	M												09-7	(2150)	(1) Diatom test	
	6	M												09-7	(2150)	(2) Angular qtz. fragment	
	6		M											09-7	(2150)	(3) Fe rich particle	
	15	M												09-7	(2150)	(4) Angular qtz. fragment	
	60													09-7	(2150)	(5) Organic fibre	
	50	M	M	I	M									09-8	(1810)	Mica flake – unweathered	
	20																Pollen grain
	30	M	M	I	T	T		I	T	T				09-9	(2610)	Clay particle showing cleavage	
	20	M	I	I	T	T		I	T	T	T	T		09-10	(1022)	(1) Silicate fragment	
	10	M	I	I	T	T		I	T					09-10	(1022)	(2) Clay mineral	
	5	M	I	I	T	T		I						09-10	(1022)	(3) Fe-rich smectite particle	
	3	M												09-10	(1022)	(4) Diatom fragment	
	15	M	M			I					I			09-10	(1022)	(5) Marine flocc.	
	100	M												09-11	(4900)	Qtz. fragment – faceted	
	100	M												09-12	(1300)	(1) organic fragment	
	30	M	M	M	T			T						09-12	(1300)	(2) rounded clay pellet	
	20			M										09-13	(3000)	(3) Fe spherule (tektite)	
10	T		M										09-14	(5500)	Fe rich rosettes on clay mineral		
50																Pollen grain	
20														09-16	(5300)	Pollen Grain	

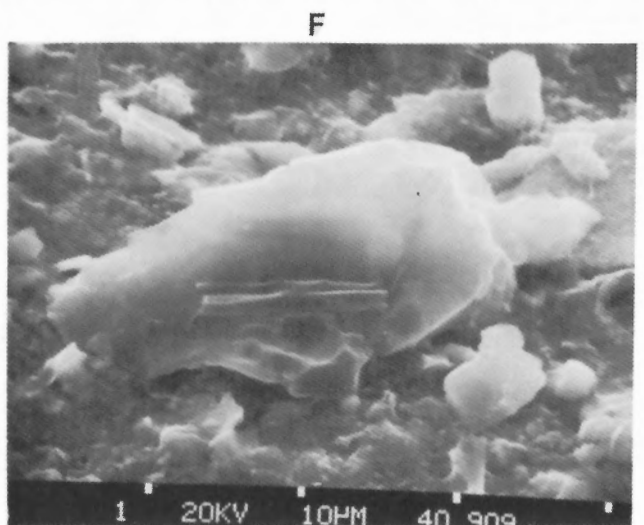
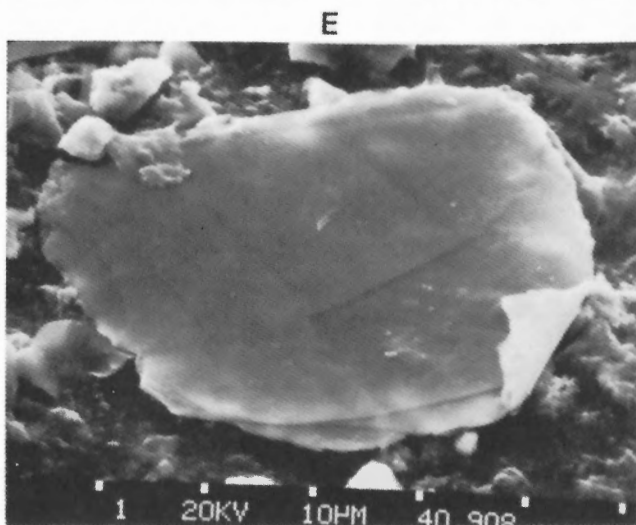
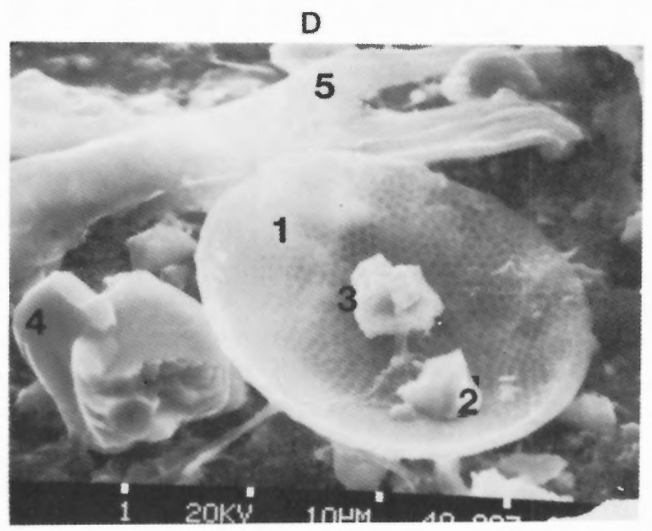
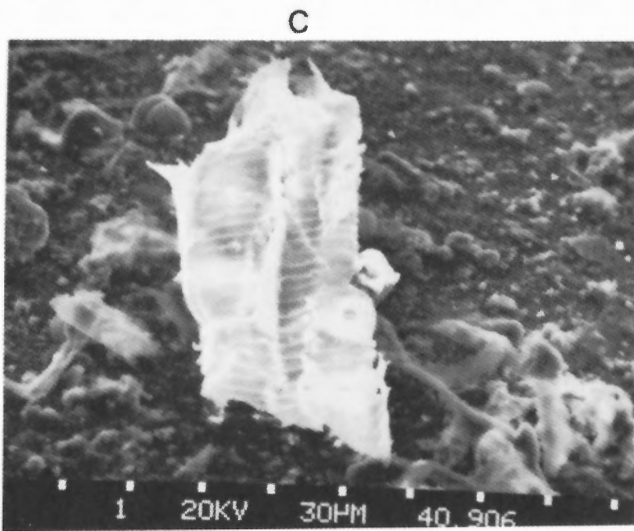
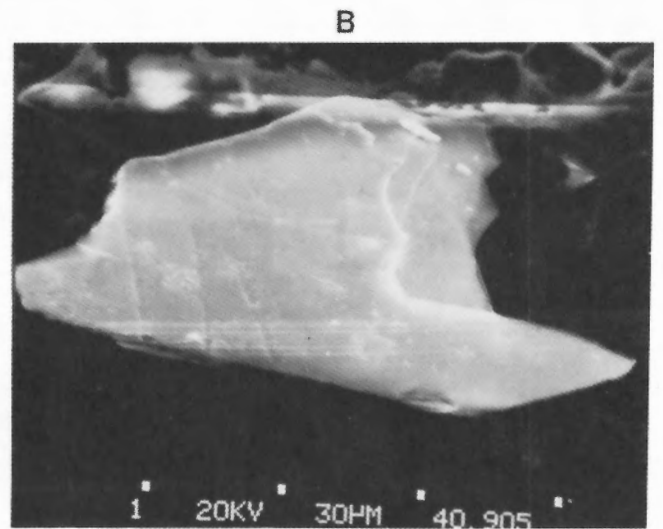
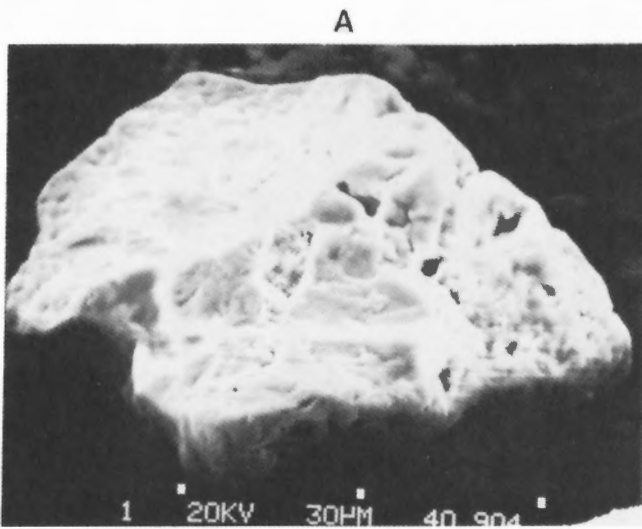


Plate 4.5

Micrographs of particulate matter from the ice pack. A, ferrosilicate clast; B, orthoclase; C, wood fibre; D, 1, diatom test, 2, quartz fragment, 3, iron-rich particle, 4, quartz fragment, 5, organic fibre; E, mica plate; F, clay particle.

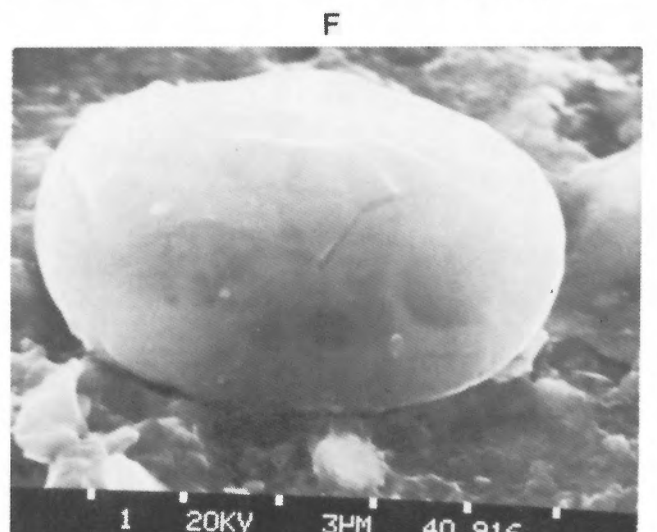
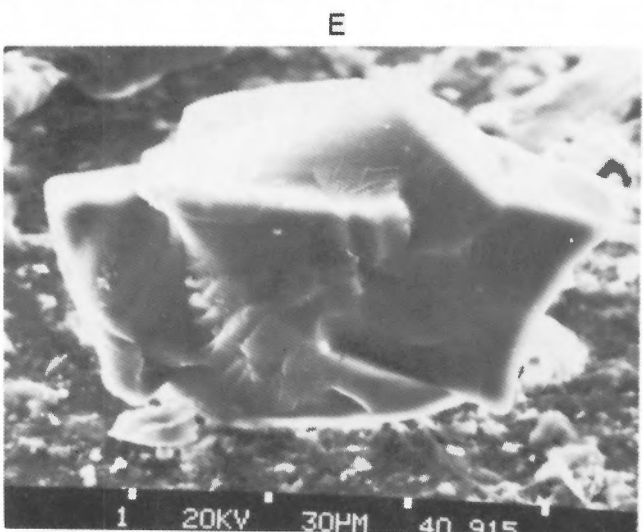
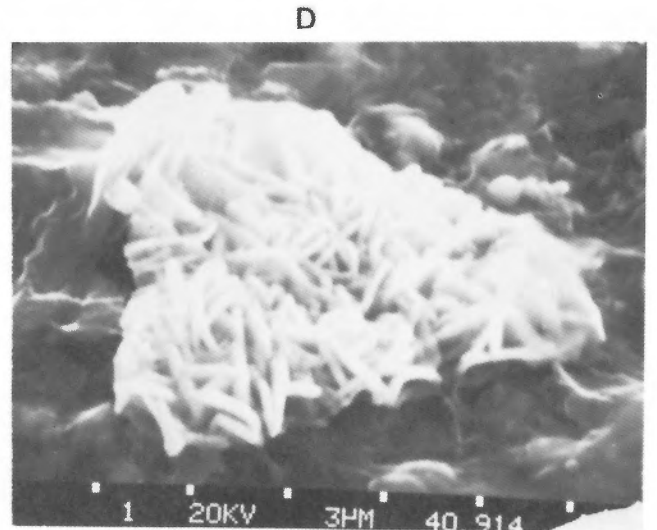
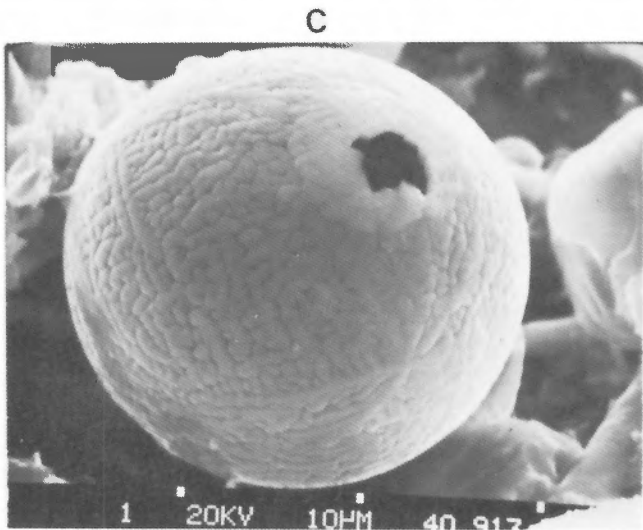
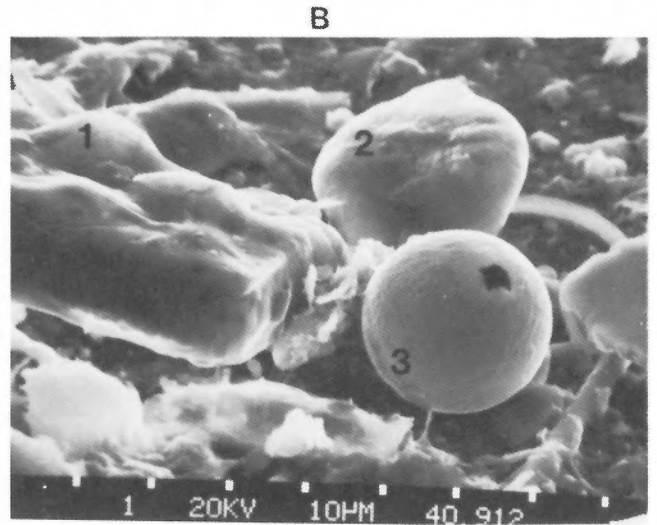
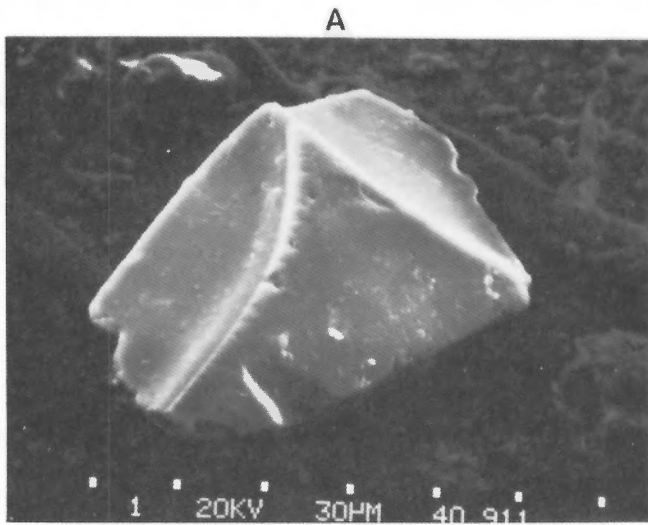


Plate 4.6

Micrographs of particulate matter from the ice pack. A, faceted quartz fragment; B, 1, organic matter, 2, rounded clay pellet, 3, iron-rich spherule (micro-meteorite); C, iron-rich spherule (micro-meteorite); D, iron-rich rosettes; E, phosphorus-rich soap (contamination resulting from use of deflocculant); F, pollen grain.

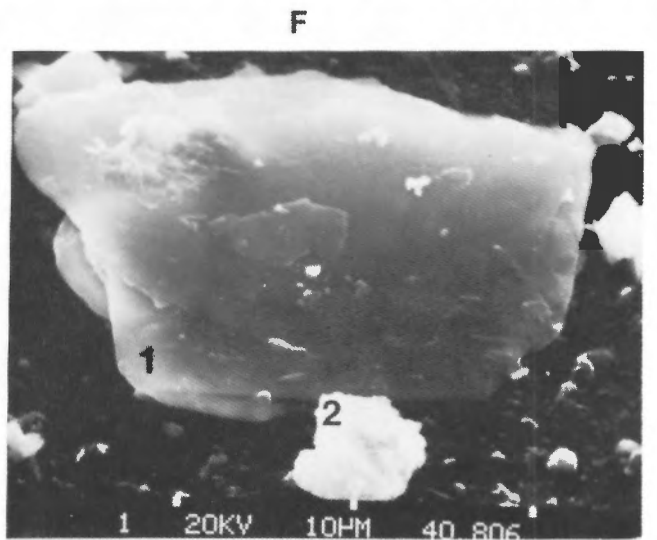
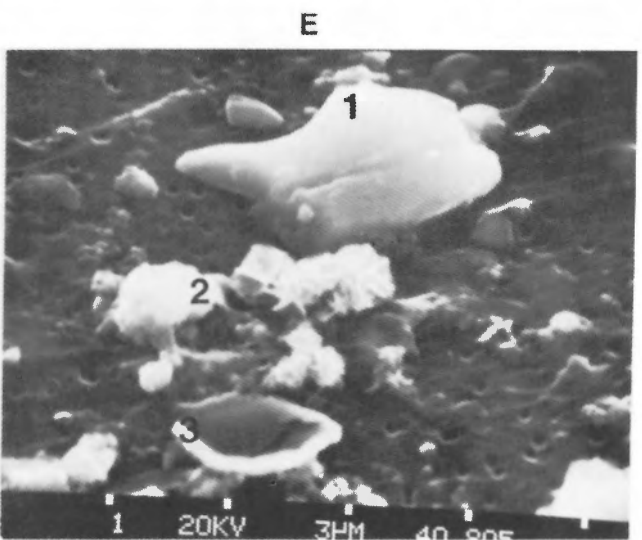
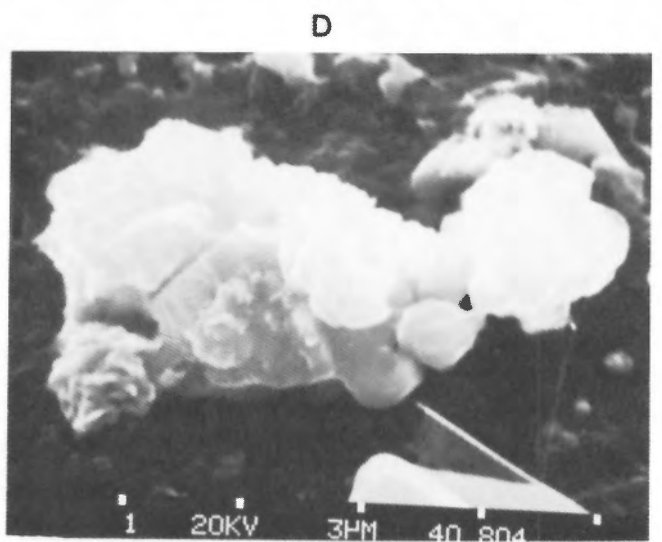
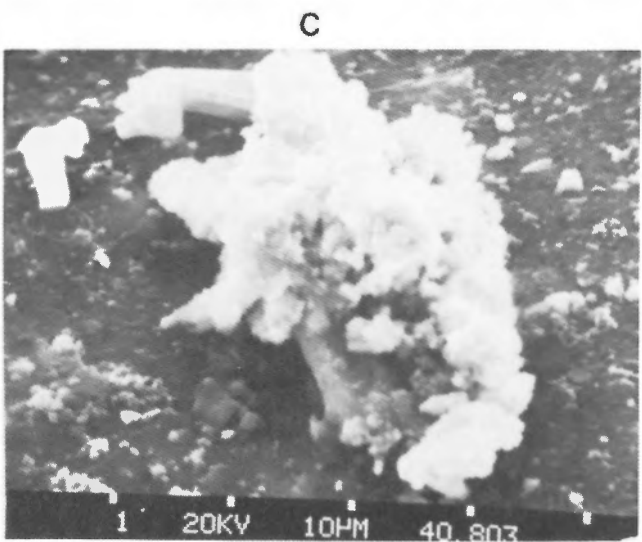
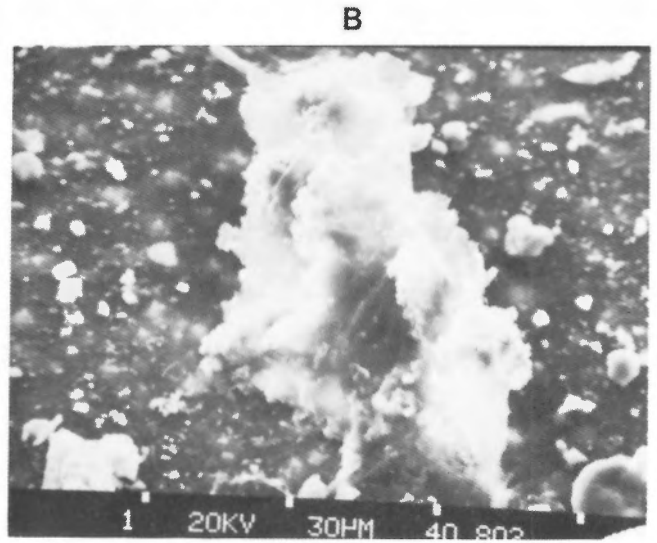
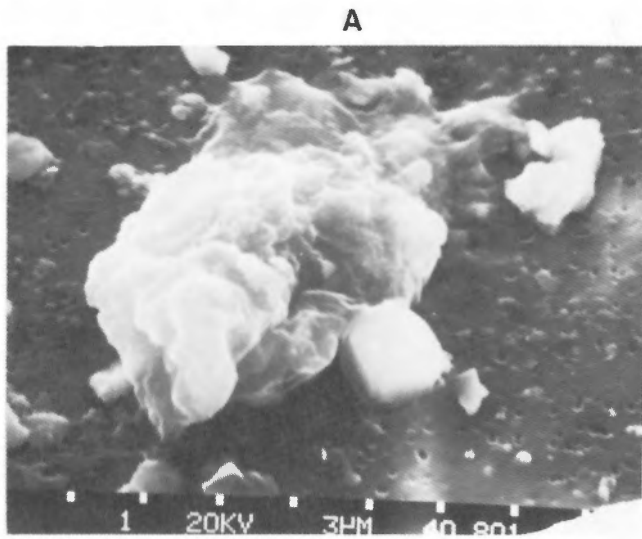


Plate 4.7

Micrographs of particulate matter from 25m water depth. A, clay (smectite) floccule; B, organic-rich clay floccule; C, organic-rich floccule; D, iron-rich smectite floccule; E.1, clay plate, 2, iron-rich particle, 3, diatom fragment; F.1, mica plate, 2, iron-rich particle.

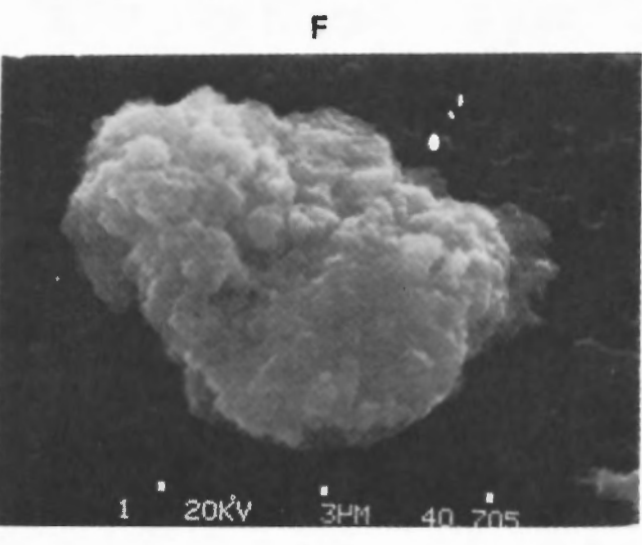
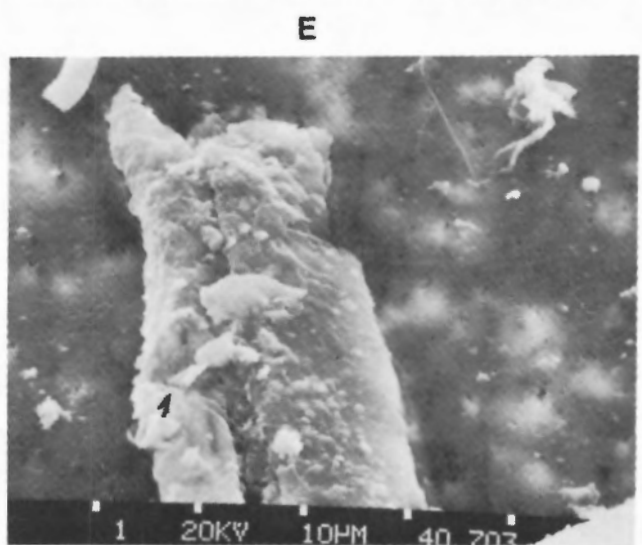
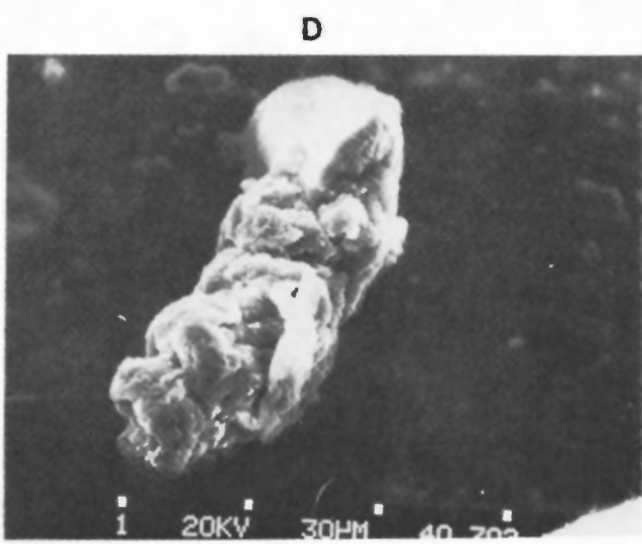
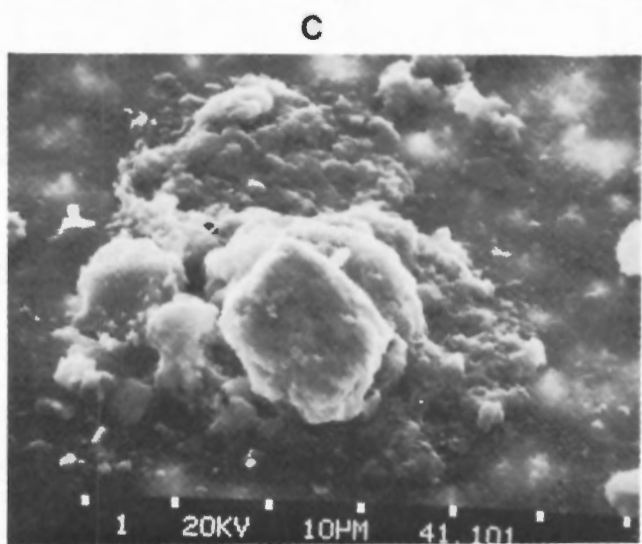
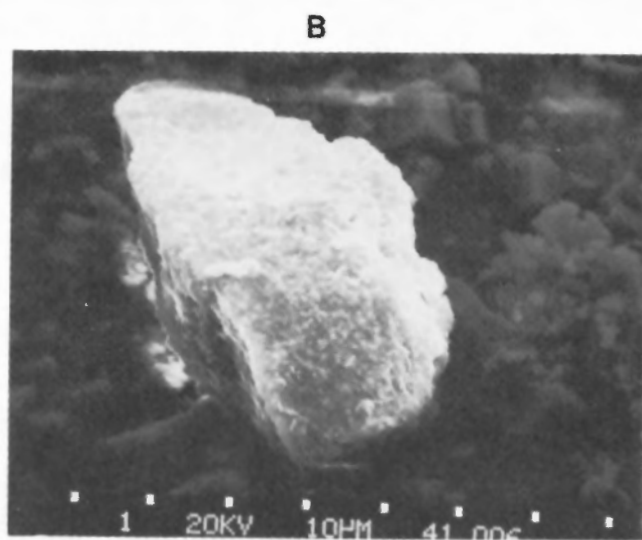
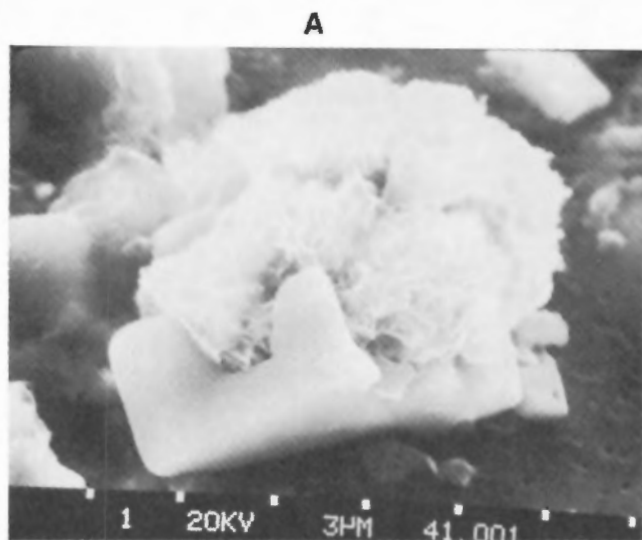


Plate 4.8

Micrographs of particulate matter from 350m (A and B), 1000m (C) and 1330m (D, E and F). A, iron-rich rosettes on salt; B, lead-rich particle (possibly crocoite); C, iron-rich floccule; D, quartz fragment; E, weathered feldspar; F, iron-rich floccule.

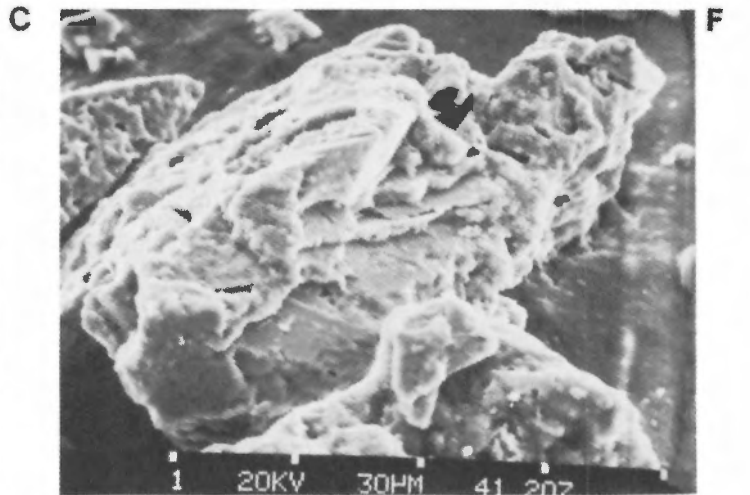
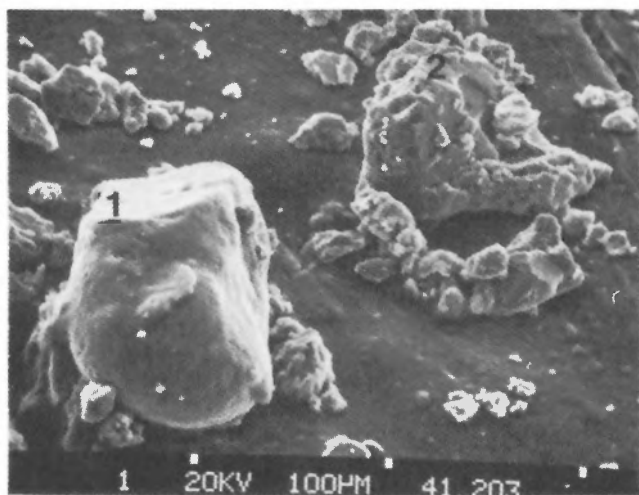
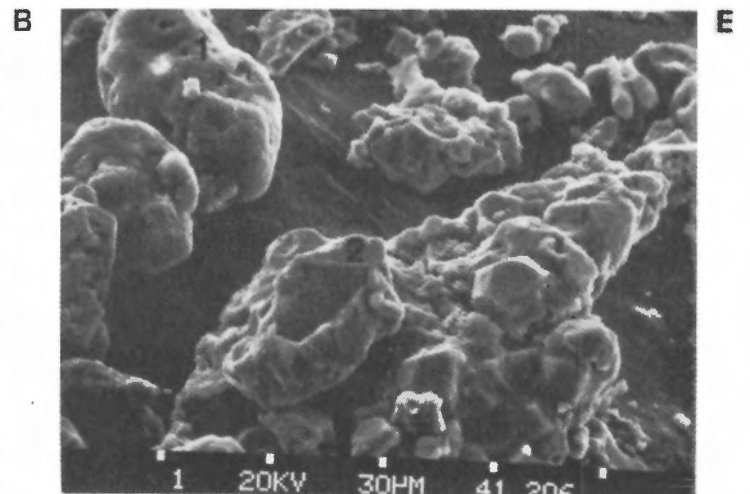
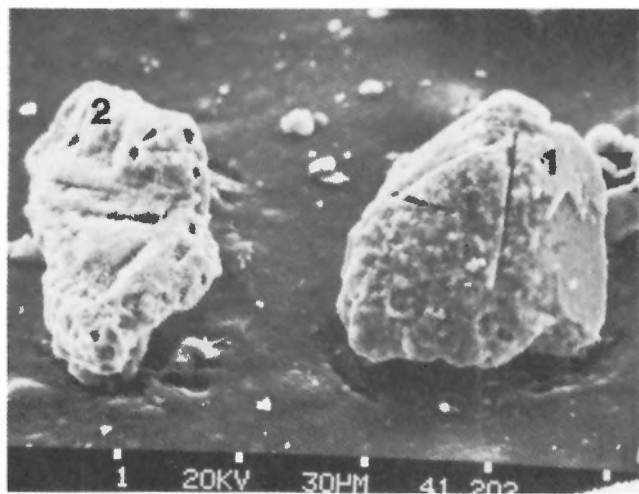
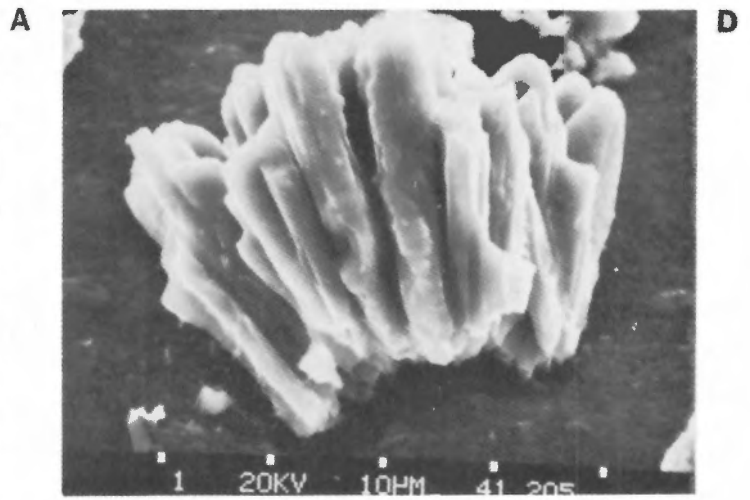
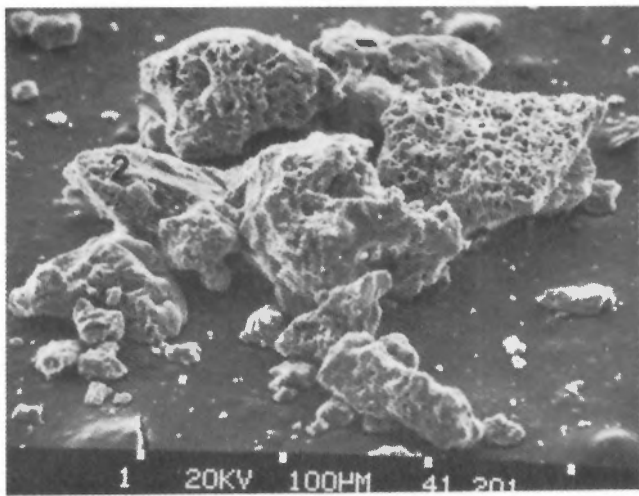


Plate 4.9

Micrographs of weathered products of bedrock sample recovered in dredge D10. A.1, iron-rich coating on clay particle; 2, feldspar crystal; B.1, cleavage planes on pseudomorph of feldspar, 2, weathered feldspar; C.1, well rounded Fe/Mn/Mg precipitate, 2, weathered feldspar; D, clean feldspar; E, rounded Fe/Mn/Mg precipitate; F, well weathered feldspar.

water column. The analysis reflected the SPM modes. That is, there is a predominance of iron-rich amorphous material (Plate 4.9A) and silica-aluminum-potassium-rich well weathered pseudomorphs (Plate 4.9B). The pseudomorphs show perfect basal and B- plane cleavage patterns and cross-sections similar to microline phenocrysts. Such crystals vary in size from 30 to 100 μ m and, if interpreted correctly, are typically associated with hydrothermal veins or pegmatites. The weathering of the pseudomorphs shows a continuum from partially leached crystals to fully altered smectite flocules. Well rounded spherules of Fe/Mg rich material were also present. The trace metals measured in these spherules were titanium and potassium with intermediate amounts of aluminum, silica and calcium. The spherules are similar in composition to the pyroxene group, although no crystal faces were observed. An alternate hypothesis is that they are amorphous concretions associated with hydrothermal activity which created the Fe/Mg rich crust covering the bedrock surface.

The following is an approximate element composition table of the bedrock crust derived from the EDAX system:

Element	%
Na	trace
Mg	13
Al	16
Si	8
K	trace
Ca	4
Ti	trace
Mn	37
Fe	19

(traces of Ni also present)

DISCUSSION

The sedimentation rate to the basins of the Alpha Ridge can be computed from a knowledge of the depth average suspended sediment concentration (SSC), from information on floccule bulk density and settling rate and by assuming no significant current flow. Accretion rate is derived from sedimentation rate assuming a bulk density for the bottom sediment of 1800kg (m³)⁻¹. Specifically, a sediment concentration of 0.01 x 10⁻³kg (m³)⁻¹ and a floccule settling rate (V₀) of 630 m.a.⁻¹ were used. The value of V₀ is based on experimental evidence.

$$\begin{aligned} \text{Accumulation rate} &= (\text{SSC}) \cdot (V_0) \cdot \left(\frac{1}{1800} \right) \text{ m.a}^{-1} \\ &= (1 \times 10^{-5}) \cdot \left(\frac{1}{1800} \right) \text{ m.a}^{-1} \\ &= 3.5 \times 10^{-3} \text{ mm.a}^{-1} \end{aligned}$$

The results show an extremely slow sedimentation rate of 1mm in approximately 300 years. Thus it would take 0.3 Ma to accumulate 1m of bottom sediment assuming normal pelagic sedimentation. Due to the pulse-like nature of eolian sediment input to the water column (which occurs during

summer ice melting) and the inferred resuspension of ridge-top sediments during seabed storms, the above calculation is considered to be conservative. Notwithstanding this, previously published data on sedimentation rates fall generally within the range specified. Herman (1974) quoted rates of 1 to 3mm (1000 a)⁻¹ as a general value for the Alpha Ridge and suggested higher rates for the adjacent plains. Clark et al. (1980), based on core data, suggested a rate of 1.14mm (1000 a)⁻¹, while Aksu (1985) derived a value of 1mm (1000 a)⁻¹.

CONCLUSIONS

Notwithstanding the incomplete data set, the following are the significant conclusions of this study.

1. The UMEL camera and frame, used originally in the AIDJAX project, is not appropriate for operations such as CESAR. A more compact system, that could be lowered directly through the hydrohole without tilting, would reduce the risks of injury or instrument damage.
2. A sum of 605 useable bottom photographs were obtained from 14 sites. The photographs showed the northern Alpha Ridge crest is current winnowed, while the troughs show evidence of tranquil sedimentation. Ripples and scouring around cobbles, observed at the ridge crest, are suggestive of periodic currents in excess of 20cm.s⁻¹.
3. The nearbed currents, interpreted from the drift rates of trigger weight impact plumes seen in bottom photographs, were approximately 1cm.s⁻¹.
4. The principal type of bottom sediment found at the ridge crest was allogenic and inorganic. By contrast, 60% of the material in the adjacent troughs was biogenic. Of the remaining inorganic sediment, the silt/clay component was principally derived from local bedrock weathering, whereas the sand/gravel population was principally derived from ice rafting of debris from adjacent land masses.
5. The majority of the particulate matter in the ice pack comprised eolian debris although marine flocs were also found. The concentration of particulate matter in the ice was an order of magnitude higher than in the water column suggesting that the sediment supply from eolian processes is greater than advection to the region within the water column.
6. Gravel clasts, recovered from the seabed and interpreted to be ice rafted to the region, are predominantly rounded to well rounded and are calcareous. This suggests a source from a beach or river delta on the adjacent Canadian land mass.
7. Bedrock material, dredged from the south flank of the northern Alpha Ridge crest, verifies the occurrence of outcrops in the region. This material is an extremely well weathered, buff basaltic rock with a surface crust of Fe/Mn rich precipitate.
8. The mean sediment concentration in the water column was 80mg.L⁻¹ (\pm 70mg.L⁻¹). A layer of micaceous rich

material was detected at a depth of 1000m, although no obvious stratification in the sediment concentration was observed.

9. A first-order calculation of sedimentation rate, using the measured sediment concentration in the water column, was 1m in 0.3 Ma. This correlates well with estimates derived by other methods.

REFERENCES

- Aksu, A.E.
1985: Paleomagnetic stratigraphy of the CESAR cores; *in* Initial Geological Report on CESAR — the Canadian Expedition to Study the Alpha Ridge, Arctic Ocean, ed. H.R. Jackson, P.J. Mudie and S.M. Blasco; Geological Survey of Canada, Paper 84-22, report 7.
- Clark, D.L., Whitman, R.R., Morgan, K.A. and MacKey, S.D.
1980: Stratigraphy and glacial-marine sediments of the American basin, central Arctic Ocean; Geological Society of America, Special Paper, 131, 57p.
- Crombie, W.J.
1960: Preliminary results of investigations on Arctic Drift Station Charlie; *in* Geology of the Arctic, ed. G.O. Raasch; University of Toronto Press, p.670-703.
- Hall, J.K.
1979: Sediment waves and other evidence of paleo-bottom current at two locations in the deep Arctic Ocean; *Sedimentary Geology*, v.23, p.269-299.
- Herman, Y.
1974: Arctic Ocean sediments, microfauna and the climatic record in late Cenozoic time; *in* Marine Geology and Oceanography of the Arctic Seas, ed. Y. Herman; Springer-Verlag, New York, p.223-348.
- Hunkins, K.L., Ewing, M., Heezen, B.C. and Menzies, R.J.
1960: Biological and geological observations on the first photographs of the Arctic Ocean deep-sea floor; *Limnology Oceanography*, v.5, p.154-160.
- Hunkins, K.L., Thorndike, E.M. and Mathieu, G.
1969: Nepheloid layers and bottom currents in the Arctic Ocean; *Journal of Geophysical Research*, v.74, p.6995-7008.
- Kamphuis, J.W. and Hall, R.
1983: Cohesive material erosion by unidirectional current; *Journal of Hydraulic Engineering, ASCE*, v.109, p.49-61.
- Middleton, G.V. and Southard, J.B.
1978: Mechanics of sediment movement; *SEPM Short Course No.3*, 10.2p.
- Piper, D.J.W., Letson, J.R.J., De Iure, A.M. and Barrie, C.Q.
1983: Sediment accumulation in low-sedimentation, wave dominated, glaciated inlets; *Sedimentary Geology*, v.36, p.195-215.
- Schwarzacher, W. and Hunkins, K.L.
1965: Dredged gravels from the central Arctic Ocean U.S.; *in* I.G.Y. drifting station Alpha Arctic Ocean 1957-1958, ed. G.H. Cabaniss, K.L. Hunkins and N. Untersteiner; Office of Aerospace Research, p.173-174.
- Van Wagoner, N.A. and Robinson, P.T.
1985: Petrology and geochemistry of a CESAR bedrock sample: implications for the origin of the Alpha Ridge; *in* Initial Geological Report on CESAR — the Canadian Expedition to Study the Alpha Ridge, Arctic Ocean, ed. H.R. Jackson, P.J. Mudie and S.M. Blasco; Geological Survey of Canada, Paper 84-22, report 5.